Available online at www.sciencedirect.com

ScienceDirect

Procedia CIRP 95 (2020) 927–932

www.elsevier.com/locate/procedia

20th CIRP CONFERENCE ON ELECTRO PHYSICAL AND CHEMICAL MACHINING

Effects of laser microtextured surfaces in condensation heat transfer

Haydee Martinez-Zavala[a], Debajyoti Bhaduri[a]*, Petko Petkov[b], Agustin Valera-Medina[a], Samuel Bigot[a]

[a]*School of Engineering, Cardiff University, Queen's Buildings, The Parade, Cardiff, CF24 3AA, UK*
[b]*School of Engineering, University of Portsmouth, Anglesea Building, Anglesea Road, Portsmouth, PO1 3DJ, UK*

* Corresponding author. Tel.: +44(0)29 2251 0922. E-mail address: BhaduriD@cardiff.ac.uk

Abstract

Some major application areas of microtextured surfaces are found in the energy, biomedical, transportation and aerospace sectors. In relation to the energy sector, microtextured surfaces provide an energy efficient and cost-effective passive mechanism for increased heat transfer during matter's phase change in energy recovery systems. This study explores the viability of laser microprocessing as an attractive manufacturing route for generating textured surfaces and compares with the results from a previous study involving microgeometries created by micro-wire electro discharge machining (μWEDM). Two types of stainless steel SS316L insert, produced via casting followed by machining, as well as by selective laser melting (SLM), were used as the workpieces. A number of microtextured geometries were produced on the workpieces' planar top faces using a nanosecond fibre laser (1064 nm wavelength) operating with 0.066 and 0.25 mJ laser energy, 10 and 80 kHz frequencies, 400, 600 and 700 mm/s beam scanning speeds, and 25 and 60 μm set distances between the unidirectional textured grooves/laser tracks. The textured surfaces were subsequently scanned using a 3D optical scanner for evaluating the depth and width of the geometries. The scanning electron micrographs showed comparable groove geometries produced via both laser and μWEDM. During condensation experiments, the laser textured surfaces typically exhibited higher differential temperature, ΔT (~11.9-28.9%) with respect to the unstructured specimens. Additionally, the textured SLM samples generally showed greater heat transfer quality (~3.7-5.7% higher ΔT) than their cast and machined counterparts.

Peer-review under responsibility of the scientific committee of the ISEM 2020

Keywords: Laser microtexturing; biologically inspired design; surface analysis; condensation; heat transfer; stainless steel

1. Introduction

Natural phenomena, from macroscale to micro and nanoscales, have inspired new materials, devices and processes due to their efficient biological design and physical and chemical properties of great commercial and industrial interest. Through biomimetics, biologically inspired microtextured surfaces have been designed to mimic properties of plants and animals. An example of this is superhydrophobicity of lotus leaves and rose petals that facilitates adhesion, self-cleaning, and drag reduction allowing water droplets to easily drain while cleaning the surface. Other instances are low hydrodynamic drag and self-cleaning properties of sharkskins, enrichment of aerodynamic lift in birds through their feather structures; high mechanical strengths of seashells; thermal insulation properties of mammal furs and skins etc [1]. Biologically inspired microtextured surfaces rely on the control of surface characteristics to obtain the desired functional performances that can be exploited in order to accomplish the same functions as their counterparts in nature do [2].

By understanding the surface phenomena in nature, the development of many advanced sectors, such as energy, electrical, electronics, biomedical, information technology, optics, tribology, biology, transportation and aerospace, can benefit from energy recovery, conversion and conservation, thermal and fluid flow control, high and reversible adhesion, and aerodynamic lift [3].

Peer-review under responsibility of the scientific committee of the ISEM 2020
10.1016/j.procir.2020.01.184

1.1. Applications of microtextured surfaces in the energy sector

Numerical and experimental studies have shown microtextured surfaces being a reliable energy-efficient and cost-effective passive mechanism for increased energy transfer during matter's phase change in recovery systems, stabilisation of flashback in swirl burners for energy production [4], reduction of energy consumption through vehicle stabilisation in aerospace, heat exchangers [5], thermal control in power plants [6], cooling [7] and boiling [8,9] heat transfer.

Microtextured surfaces in heat transfer phenomena are particularly used for spray cooling and boiling mechanisms. Many authors have investigated their effects in increasing the coolant-solid contact area and the critical heat flux (CHF) in the past 50 years due to their industrial and domestic relevance [2]. Spray cooling is very efficient for dissipating high heat fluxes in supercomputing and on-board flight system components since vapour produced at the surface by phase change can be easily removed from the surface due to its high CHF. On the other hand, boiling is used to transmit thermal power through the creation of vapour bubbles in nucleation sites on the heating surface of vaporisers [2].

Over the past decades, significant progress on surface texturing, either by additive or subtractive method, has been made since it is a recognised viable option to improve surface properties. For experimental studies on boiling heat transfer, Kang and Wang [9] fabricated different geometries on the surfaces of 316L stainless steel specimens via metallic 3D microprinting via selective laser sintering (SLS). Previous experiments by the authors involving microtextured surfaces, created by micro-wire electro discharge machining (μWEDM) on 316L stainless steel specimens, exhibited a 21% higher differential temperature (ΔT) during phase change, compared to the unstructured surfaces [10]. However, according to Etsion [11], laser surface texturing (LST) is by far the most advanced technology among all other techniques that have been employed for surface texturing.

1.2. Applications of microtextured surfaces during condensation phenomenon

Although the use of microtextured surfaces has been explored both in academia and industry over the past decades as a reliable passive mechanism for enhancing heat transfer during cooling and boiling, research on the effects of these surfaces during condensation heat transfer is rather limited.

Condensation heat transfer is a phenomenon commonly seen in engineering processes such as refrigeration and power generation [12] and can take place via two mechanisms depending on the wettability of the surface: Dropwise Condensation (DWC) in non-wettable surfaces and Filmwise Condensation (FWC) in wettable surfaces. Dropwise condensation is based on the stages of a droplet life cycle: nucleation, growth, and departure; while in filmwise condensation a film of condensate is formed, which implies a lower heat transfer effect due to the resistance of the liquid film thickness between the environment and the surface.

By altering the physical structure of the surface, rapid droplet removal, which plays a major role on the heat transfer during condensation, can be accelerated [13]. Orejon et al. [14] demonstrated that simultaneous DWC/FWC provides a good heat transfer performance by varying the microtextured surfaces' design parameters, while Qi et al [12] demonstrated that the used of grooved surfaces decreases liquid film thickness.

1.3. Aim and objective

The aim of this study is to explore an alternative manufacturing route for generating microtextured surfaces via laser microprocessing technology which can offer some intrinsic benefits over μWEDM, with the objective of enhancing condensation heat transfer between the large latent heat in humid systems and an energy recovery device.

2. Experimental details

2.1. Insert manufacturing process

Two types of stainless steel (grade 316L) inserts were manufactured via casting followed by conventional turning and facing operations (CM), as well as by selective laser melting (SLM). The SLM process utilised SS316L powders of ~15-45 μm average particle size, a 200 W laser power, with a beam spot size of 56 μm (Gaussian profile) and layer thickness of 50 μm. The point distance between two consecutive laser beam spots was 60 μm with a laser exposure time of 80 μs while the hatch distance was set at 110 μs. The height of the inserts was 25 mm while the bottom 10 mm had a diameter of 28 mm and the top 15 mm had a diameter of 25 mm (Fig. 1 a).

2.2. Microtexturing process

Laser microprocessing, a faster, cleaner and more flexible manufacturing technique was selected over μWEDM to produce different geometries on CM and SLM inserts. First, the top faces (of 25 mm diameter) of the CM inserts were machined (roughness R_a = 0.2 μm) prior to laser microtexturing. The SLM top faces were pretreated with a nanosecond fibre laser (1064 nm wavelength) to reduce surface asperities for the laser microtexturing stage.

The microgeometries were then generated on the planar top faces of both types of insert using the same laser source but with different laser energies (0.066 and 0.25 mJ), frequencies (10 and 80 kHz), beam scanning speeds (400, 600 and 700 mm/s) and set distances between the unidirectional textured grooves/laser tracks (25 and 60 μm). A pulse width of 65 ns and a Gaussian beam profile with a focal spot size of 32 μm were used in all tests.

2.3. Experimental specimens

In summary, two preliminary scallop inspired geometries (A and B) and two superhydrophobic geometries (C and D) were manufactured by laser microprocessing on specimens manufactured via casting followed by machining (CM) and via selective laser melting (SLM): CL-A, CL-B, CL-C, CL-D, SLM-A, SLM-C, and SLM-D.

2.4. Characterisation of the microtextured surfaces

An optical 3D scanner 'Sensofar Smart' was employed for scanning the scallop inspired geometries (CL-A, SLM-A and CL-B). For the characterisation, five areas of dimension 1.7 mm × 1.4 mm were scanned on the structured 25 mm inserts' top surface, the approximate locations of which are shown in Fig. 1b. Each of the scanned areas was divided into three sections from where five measurement points were chosen as seen in Fig. 1c. Then at each point, four different groove characteristics were measured: width of the groove, width of the riblet, pitch and depth of the groove at the approximate locations in Fig. 1d. Due to the complex geometry presented on the superhydrophobic surfaces, a scanning electron microscope (SEM) was employed to obtain the visual representations of the specimens CL-C, SLM-C, CL-D, and SLM-D; the images shown in Fig. 4.

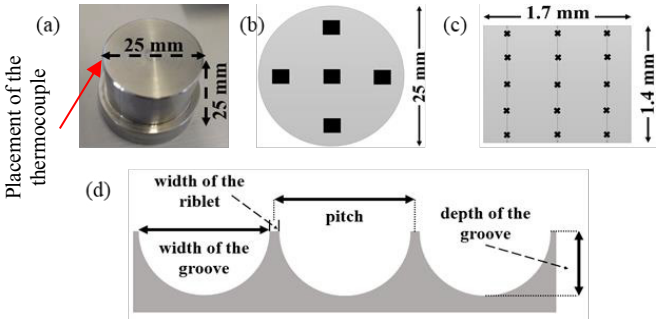

Fig. 1. (a) Unstructured insert manufactured via casting followed by machining, and representations of (b) an insert's top surface; (c) a scanned area; and (d) locations of the grooves' measured characteristics.

2.5. Condensation experiments

For the experimental phase the following arguments were taken into consideration: (1) The rate of heat transfer (Q) is directly proportional to the differential temperature (ΔT). Hence ΔT was chosen as the main parameter in this study to analyse the effect of laser microtextured surfaces in condensation heat transfer. (2) The humid flow velocity entering the condensation chamber is very low (0.15 m/s), thus the interfacial shear between the liquid and the vapour is negligible [12]. (3) Considering that the phenomenon occurs under humid environments, the temperature and relative humidity in the condensation chamber were set-up to 303.33 K ± 0.72% and 90.77 ± 11.88 %RH, according to the statistical analysis and collection of data by The National Oceanic and Atmospheric Administration (NOAA) [15].

The specimens were completely insulated with waterproof insulating tape while leaving the top surface open for testing. The thermocouples for the temperature measurement were placed inside the insulating area, right at the edge between the top and side faces (shown by the red arrow in Fig. 1a). Temperature and %RH measurements inside the chamber and the inserts' surface temperatures were recorded every 10 seconds. The experimental apparatus is shown in Fig. 2, and the details of the components are available in Martinez-Zavala et al. [10], with an upgrade in the thermocouple data logger [16].

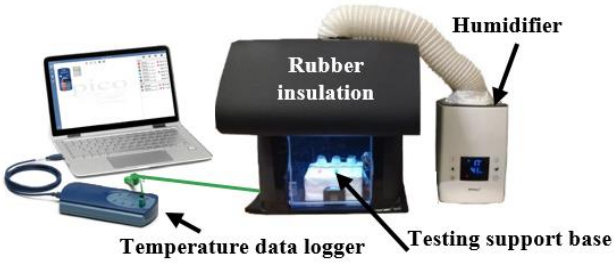

Fig. 2. Experimental apparatus for the condensation heat transfer experiments [10,16].

3. Results and Discussion

3.1. Characterisation of the microtextured surfaces

The characterisation scans obtained with Sensofar Smart for all the specimens are shown in Fig. 3. For the scallop inspired specimens (CL-A, SLM-A, and CL-B) a 10X objective was used to scan an area of 1.7 mm × 1.4 mm. Furthermore, in order to compare the LST's effect on condensation, previous results obtained by the authors [10] using a scallop inspired specimen produced via micro-wire electro discharge machining (μWEDM) is included in Fig. 3 as "CW*". The averages of the measured data for each groove characteristic of the scallop specimens are presented in Table 1. For the superhydrophobic specimens (CL-C, SLM-C, CL-D, and SLM-D), a 50X objective was employed for scanning a 0.34 mm × 0.28 mm area. Nevertheless, quantitative surface characteristic data could not be obtained for the superhydrophobic geometries due to the surface irregularities, as seen in Fig. 3 (e-h). For this reason, a scanning electron microscope (SEM) was used for magnified images of the superhydrophobic as well as the scallop inspired specimens (Fig. 4).

Although specimens CL-A and SLM-A's surfaces were textured using the same laser parameters, as per the measured data from the Sensofar 3D profiler, there is a 4.54% difference in the widths of the grooves, a 31.36% difference in the widths of the riblets, a 15.64% variation in the pitches and a 0.39% difference in the depths of the grooves.

Table 1. Characterisation data for the CL-A, SLM-A, CL-B and CW* specimens.

Specimen	Width of the groove (μm)	Width of the riblet (μm)	Pitch (μm)	Depth of the groove (μm)
CL-A	65.36	46.08	111.44	223.80
SLM-A	68.33	60.53	128.87	224.68
CL-B	60.97	48.49	109.47	185.71
CW*	101.56	26.53	128.09	75.63

For the SEM images (Fig. 4) an magnification of 500X was used for all specimens (b-g). For enlarged views of each type of geometry, a 4000X magnification was utilised for the scallop specimen (a) while a 1000X magnification was employed for the superhydrophobic sample (g).

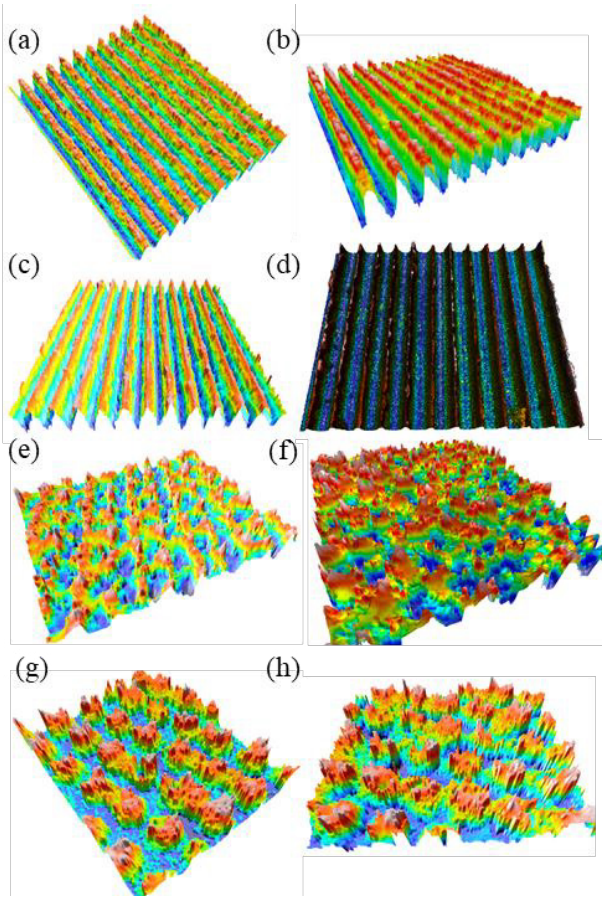

Fig. 3. Scanned surface topographies obtained via 3D optical profiler (a) CL-A, (b) SLM-A, (c) CL-B, (d) CW* (area 1.7 mm × 1.4 mm) and (e) CL-C, (f) SLM-C, (g) CL-D, and (h) SLM-D (area 3.4 mm × 2.8 mm).

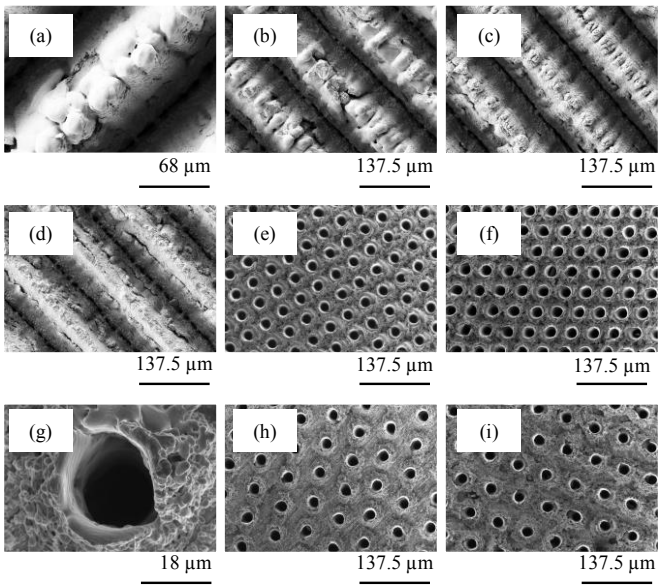

Fig. 4. Scanning electron microscope (SEM) images of (a) CL-A, (b) CL-A, (c) SLM-A, (d) CL-B, (e) CL-C, (f) SLM-C, (g) CL-D, (h) CL-D, (i) SLM-D.

3.2. Condensation experiments

The differential temperature (ΔT) in the scallop inspired geometries SLM-A, CL-A and CL-B was 28.99%, 24.41% and 23.81%, while the ΔT in the superhydrophobic geometries SLM-C, CL-C, SLM-D, and CL-D was 22.54%, 24.06%, 18.90% and 11.89% higher than the unstructured surface, respectively (Table 2). The highest ΔT (2.51 K) was observed for the SLM-A geometry with a 28.99% enhancement. In two of three cases, the SLM specimens (A and D) exhibited better performances than their CL counterparts (~3.7-5.7% higher ΔT). Results are compared with the previous experimental data reported in [10]. An enhancement in condensation heat transfer by 21.05% and 26.32% were observed when using scallop and diamond geometries manufactured via µWEDM (CW*) [10]. Other numerical and experimental results showed an improvement in heat transfer by 20 and 50% when evaluating hydrophobic and hydrophilic patterned grooved surfaces by Qi et al. [12] and Chatterjee et al. [13].

Table 2. Differential temperature (ΔT) results, together with standard errors of mean and improvement percentages (%).

Specimen	ΔT (K)	Standard error of mean	Improvement (%)
SLM-A	2.51	0.23	28.99
CL-A	2.42	0.14	24.41
CL-C	2.41	0.25	24.06
CL-B	2.41	0.12	23.81
SLM-C	2.38	0.16	22.54
SLM-D	2.31	0.12	18.90
CL-D	2.18	0.08	11.89
Unstructured	1.94	0.19	-

Figure 5 shows the images of each specimen's effect on the condensate. Dropwise condensation was observed on the microtextured surfaces since it was possible to visualise different stages of the droplet life cycle after 8 minutes during the experiment. Nucleation on (e) SLM-C; (f) SLM-D; (g) CL-D; and (h) unstructured specimens, growth on (b) CL-A; (c) CL-C; and (d) CL-B samples and departure on (a) SLM-A insert are visible in Fig. 5. The fact that the scallop specimens presented a higher droplet removal and smaller droplet size could in part explain the higher ΔT observed for the scallop specimens in this study. A higher frequency of condensate removal reduces the likelihood of droplets sticking onto the surface which significantly increases the interaction between the humid air and the surface, thus promotes the enhancement of heat transfer [17,18]. Additionally, an inversely proportional relationship between the droplet size and the ΔT was observed during the experiments which is consistent with the studies conducted by Chatterjee et al. [13], Peng et al. [19,20] and Xu et al. [21] on dropwise condensation heat transfer. Figure 6 shows the comparison between all the differential temperatures (ΔT) exhibited by the different specimens within a period of 8 minutes. Each of the curves presented in Fig. 6 is then individually analysed in Fig. 7 in order to define the number of droplet life cycles in each specimen. In the droplet life cycle, during the nucleation stage, a greater interaction between the humid air and the microtextured surface is observed leading to a higher change in the temperature. Just before the last stage, departure, the trend of temperature rise again changes. These

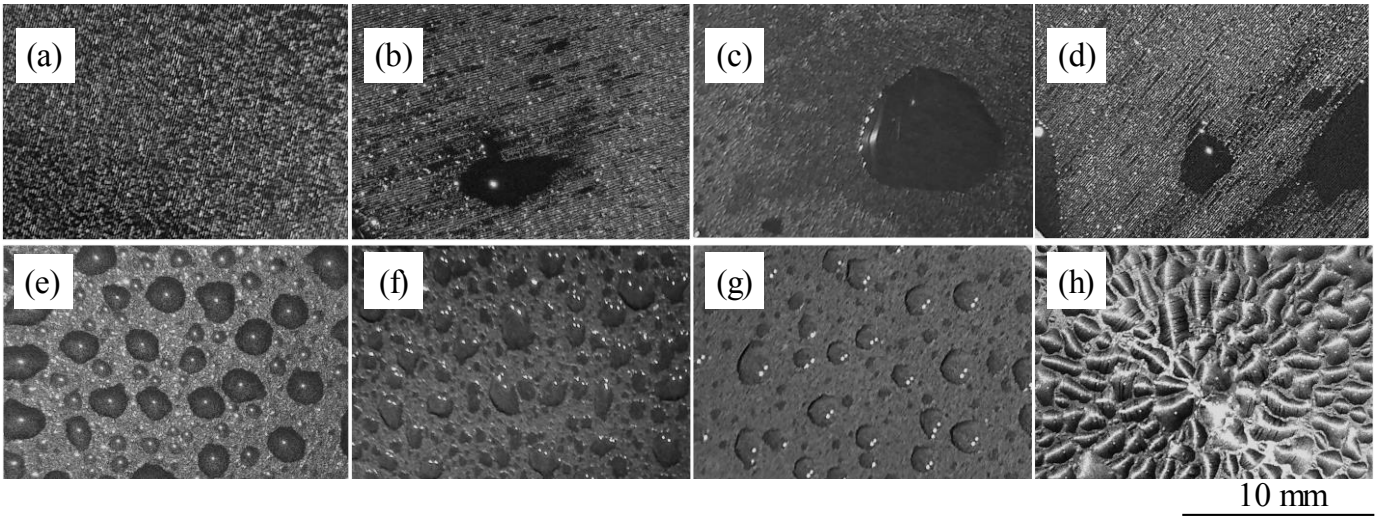

Fig. 5. Condensate on different microtextured geometries at 8th min of the experiment: (a) SLM-A; (b) CL-A; (c) CL-C; (d) CL-B; (e) SLM-C; (f) SLM-D; (g) CL-D; (h) Unstructured.

variations in the differential temperature help identifying the cycles, marked by red arrows in Fig. 7. For example, the unstructured, SLM-A, and SLM-C exhibit subtle changes throughout the experimental period and gradual and stable ΔT trends that ensure easy identification of the cycles whereas CL-A, CL-B, CL-C, SLM-D and CL-D have various deviations within the same cycle that hinder their delimitations. These could explain why SLM-A and SLM-C had a better performance than their CL counterparts. During the 8-min experiments, SLM-D exhibited 5.5 droplet life cycles while CL-D displayed ~4.5 cycles. CL-A and CL-C had 5 cycles and the rest of the specimens (SLM-A, CL-B, and SLM-C) showed 4 completed droplet life cycles.

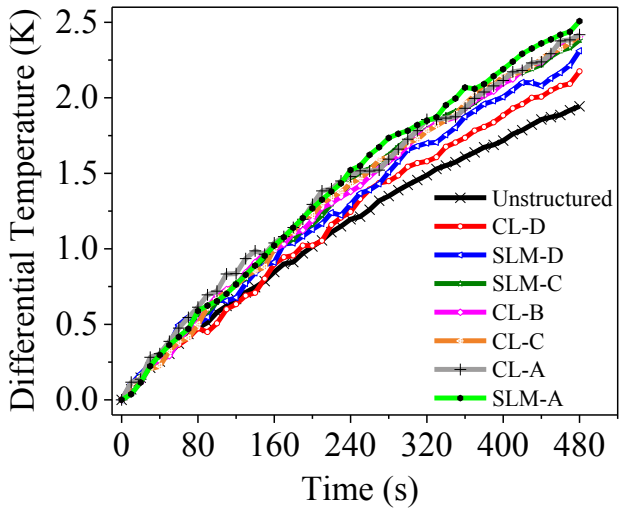

Fig. 6. Differential temperature (ΔT) vs. time.

4. Conclusions

- The scallop textures showed a more regular pattern, which facilitated the surface characteristics measurements. In contrast, the irregularities in the hydrophobic geometries, random cauliflower formations due to the rapid melting and re-solidification of the material, posed their characterisation difficult. It will be also challenging to model these hydrophobic geometries for the prediction of surface characteristics. Additionally, the insert manufacturing process might also have an effect during the phase change since 66.66% of specimens manufactured by selective laser melting (SLM) exhibited better performance than their counterparts manufactured via casting followed by machining (CM).

- Experimental data demonstrated that the differential temperatures were higher for all the laser microtextured surfaces with a scallop geometry (SLM-A), exhibiting 1.29 times higher ΔT compared to the unstructured specimen and 6.61% ΔT enhancement when compared to the µWEDM counterpart. Furthermore, the depths of the grooves generated in the inserts via laser processing were greater than that created by µWEDM, thereby increasing the contact surface area for heat transfer in the former scenario. The experimental results show similar tendencies that are reported in previous experimental and numerical studies which suggest various micro geometries can provide a higher removal of droplets to improve condensation heat transfer.

- Nonetheless, further research on laser microtexturing for condensation enhancement in humid environments for energy recovery purposes is recommended to ensure the successful consistency of the findings.

Acknowledgements

The research was supported by The Mexican National Council on Science and Technology (CONACYT) and The Secretariat of Energy in Mexico (SENER) [Grant Number 327757/460766] as part of the PhD project ‘High Peak, Perishable Energy Recovery - Foundation Phase’. Special acknowledgement is due to Mr Anuraag Saxena (CEng and MCIBSE) for his role in the construction of the experimental apparatus for the condensation heat transfer experiments.

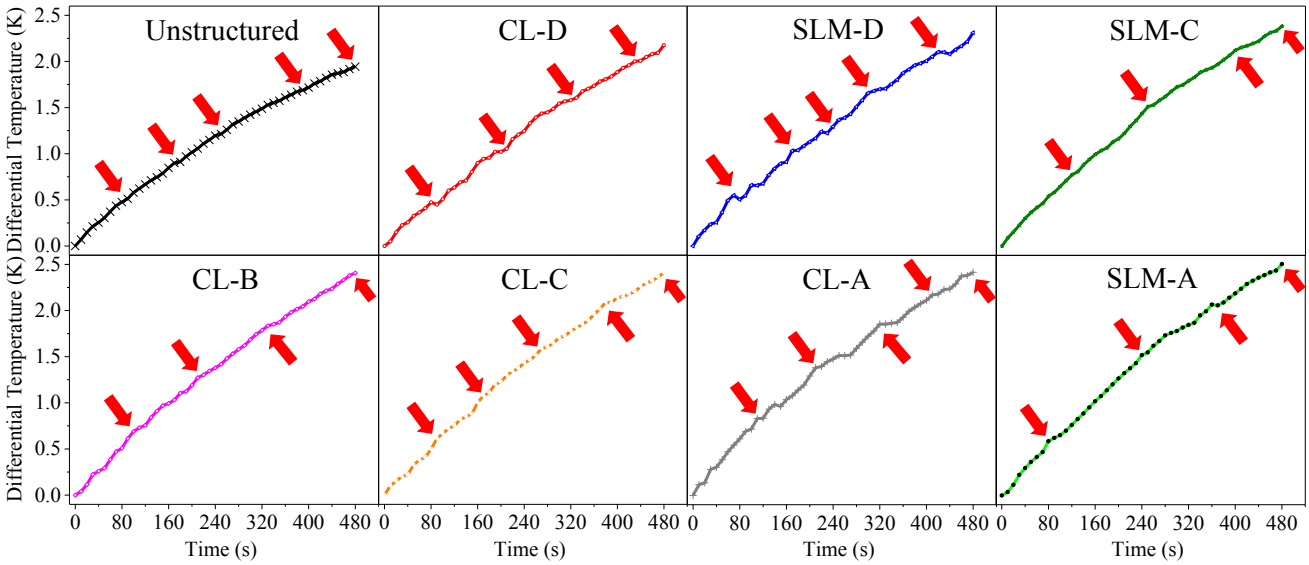

Fig. 7. Droplet life cycles for each type of textured and unstructured specimens (Unstructured, SLM-A, CL-A, CL-B, SLM-C, CL-C, SLM-D, and CL-D).

References

[1] Dean B, Bhushan B. Shark-skin surfaces for fluid-drag reduction in turbulent flow: a review. Philos Trans R Soc A Math Phys Eng Sci 2010;368:5737–5737. doi:10.1098/rsta.2010.0294.

[2] Bruzzone AAG, Costa HL, Lonardo PM, Lucca DA. Advances in engineered surfaces for functional performance. CIRP Ann - Manuf Technol 2008;57:750–69. doi:10.1016/j.cirp.2008.09.003.

[3] Bhushan B. Biomimetics: lessons from nature – an overview. Philos Trans R Soc A Math Phys Eng Sci 2009;367:1445–86. doi:10.1098/rsta.2009.0011.

[4] Al-fahham MAH. A Modelling and Experimental Study to Reduce Boundary Layer Flashback with Microstructure. Cardiff University, 2017.

[5] Brandner JJ, Anurjew E, Bohn L, Hansjosten E, Henning T, Schygulla U, et al. Concepts and realization of microstructure heat exchangers for enhanced heat transfer. Exp Therm Fluid Sci 2006;30:801–9. doi:10.1016/j.expthermflusci.2006.03.009.

[6] Zheng S, Eimann F, Philipp C, Fieback T, Gross U. Modeling of heat and mass transfer for dropwise condensation of moist air and the experimental validation. Int J Heat Mass Transf 2018;120:879–94. doi:10.1016/j.ijheatmasstransfer.2017.12.059.

[7] Renfer A, Tiwari MK, Tiwari R, Alfieri F, Brunschwiler T, Michel B, et al. Microvortex-enhanced heat transfer in 3D-integrated liquid cooling of electronic chip stacks. Int J Heat Mass Transf 2013;65:33–43. doi:10.1016/j.ijheatmasstransfer.2013.05.066.

[8] Kima SH, Lee GC, Kang JY, Moriyama K, HwanKim M, Park HS. Boiling heat transfer and critical heat flux evaluation of the pool boiling on micro structured surface. Int J Heat Mass Transf 2015;91:1140–7.

[9] Kang Z, Wang L. Boiling heat transfer on surfaces with 3D-printing microstructures. Exp Therm Fluid Sci 2018;93:165–70. doi:10.1016/j.expthermflusci.2017.12.021.

[10] Martinez-Zavala H, Bhaduri D, Valera-Medina A, Bigot S. Experimental study on heat transfer enhancement during condensation using microstructured surfaces. Int. Conf. Appl. Energy 2019, 2019.

[11] Etsion I. State of the art in laser surface texturing. J Tribol Asme 2005;127:248–53.

[12] Qi B, Wei J, Li X. Enhancement of condensation heat transfer on grooved surfaces: Numerical analysis and experimental study. Appl Surf Sci 2017;115:1287–97.

[13] Chatterjee A, Derby MM, Peles Y, Jensen MK. Enhancement of condensation heat transfer with patterned surfaces. Int J Heat Mass Transf 2014;71:675–81. doi:10.1016/j.ijheatmasstransfer.2013.12.069.

[14] Orejon D, Shardt O, Gunda NSK, Ikuta T, Takahashi K, Takata Y, et al. Simultaneous dropwise and filmwise condensation on hydrophilic microstructured surfaces. Int J Heat Mass Transf 2017;114:187–97. doi:10.1016/j.ijheatmasstransfer.2017.06.023.

[15] Cione JJ. The Relative Roles of the Ocean and Atmosphere as Revealed by Buoy Air–Sea Observations in Hurricanes. Mon Weather Rev 2014;143:904–13. doi:10.1175/mwr-d-13-00380.1.

[16] PICO Technology. 8-channel thermocouple data logger (USB TC-08). St. Neots: 2018.

[17] Anand S, Rykaczewski K, Bengaluru Subramanyam S, Beysens D, Varanasi KK. How droplets nucleate and grow on liquids and liquid impregnated surfaces. Soft Matter 2015;11:69–80. doi:10.1039/c4sm01424c.

[18] Grooten MH, Geld CW. The importance of drainage in dropwise condensation from flowing air–steam mixtures. 14th Int. Heat Transf. Conf., 2010, p. 51–60.

[19] Peng B, Ma X, Lan Z, Xu W, Wen R. Analysis of condensation heat transfer enhancement with dropwise-filmwise hybrid surface: Droplet sizes effect. Int J Heat Mass Transf 2014;77:785–94. doi:10.1016/j.ijheatmasstransfer.2014.05.052.

[20] Peng B, Ma X, Lan Z, Xu W, Wen R. Experimental investigation on steam condensation heat transfer enhancement with vertically patterned hydrophobic-hydrophilic hybrid surfaces. Int J Heat Mass Transf 2015;83:27–38. doi:10.1016/j.ijheatmasstransfer.2014.11.069.

[21] Xu W, Lan Z, Liu Q, Du B, Ma X. Droplet size distributions in dropwise condensation heat transfer: Consideration of droplet overlapping and multiple re-nucleation. Int J Heat Mass Transf 2018;127:44–54. doi:10.1016/j.ijheatmasstransfer.2018.07.020.